Electronic Supplementary Material (ESI) for Soft Matter.

Electronic Supplementary Information for:

Tuning Polyelectrolyte Multilayer Structure by Exploiting Natural Variation in Fucoidan Chemistry

*Tracey T.M. Ho [1], Kristen E. Bremmell [2], Marta Krasowska [1], Damien N. Stringer [3], Benjamin Thierry [1], and David A. Beattie [1]**

[1] Ian Wark Research Institute, University of South Australia, Mawson Lakes Campus, Mawson Lakes, SA 5095

[2] School of Pharmacy and Medical Sciences, University of South Australia, City East Campus, North Terrace, Adelaide, SA 5000

[3] Marinova Pty Ltd, 249 Kennedy Drive, Cambridge, TAS 7170, Australia

***** Corresponding author: David.Beattie@unisa.edu.au

Zeta Potential Measurements

The zeta potential value for each stage of formation of the $(FV/CH)_{10}$ and $(UP/CH)_{10}$ multilayers is given in Figure S1.

A silicon wafer was affixed at the end of a cylinder sample holder and was dipped into polyelectrolyte solution for 15 min followed by dipping in 0.1 M KCl at pH 6 for 5 minutes. The sample was then rinsed with 0.1 M KCl at pH 6 followed by rinsing in 0.001 M KCl at pH 6[a]. The sample holder with the attached sample was then mounted into the ZetaSpin apparatus, 1 mm above the reference electrode. The measurements were performed in 0.001 M KCl at pH 6. In order to avoid unsteady drift during sample rotation, the sample rotation rate (3000 RPM) was modulated by a square wave. The measured streaming potential is the jump in the voltage recorded as the motor switches the sample rotations from off to on and back off again. The streaming potential was the average taken from 10 subsequent cycles. The zeta potential, ζ, was determined using the following formula [b] [1]:

$$\zeta \cong \frac{1.96\kappa\nu^{1/2}}{\varepsilon a\Omega^{3/2}} \frac{1}{2\left(1-\frac{z}{a}-\frac{1}{2\left(\frac{z^2}{a^2}+1\right)^{1/2}}\right)} \phi_s \qquad (1)$$

where: κ – is the liquid conductivity, ν is the kinematic viscosity, ε is the liquid permittivity, a is the disc (sample) diameter, Ω is the sample rotation rate (in radians per second), z is the distance between the sample and the reference electrode and ϕ_s is the streaming potential.

The sample was then dismounted and immersed into solution of the oppositely charged polyelectrolyte and, after adsorption and rinsing steps, the streaming potential was measured again. All the steps were repeated until measurements were made for the desired number of layers adsorbed on the silicon wafer discs. There was no observation of zeta potential decrease during the 10 measurements made for each stage of the multilayer formation, indicating that the multilayers were stable during the spinning of the disc.

The first measurement point is for the native oxide layer on the silicon wafer substrates – and is approximately -75 mV. This value is consistent with measurements made for silicon oxide substrates at electrolyte strength of $1x10^{-3}$ M and pH 6 [2], determined via flat plate streaming potential. The second measurement point is for the adsorption of the branched PEI. It can be seen that the substrate undergoes charge reversal upon adsorption of the PEI, with a very large value obtained for the zeta potential (approx. 80 mV).

For $(FV/CH)_{10}$, the build-up of the multilayer from this point follows a classic saw-tooth profile, with the change in sign of zeta potential accompanying each stage of the adsorption: negative, and between -32 and -40 mV for adsorption of the fucoidan; positive and approx. 30 mV for adsorption of the chitosan. The zeta potential values have a small degree of variation during the formation of the first 5 bilayers, but after that the measured values upon adsorption of each polymer are constant. The dataset for $(UP/CH)_{10}$ is similar to that seen for $(FV/CH)_{10}$, with a few subtle differences. The value of the zeta potential for the silicon substrate and the first PEI layer are near identical to those

[a] The rinse in 0.001 M KCl at pH 6 has been performed in order to avoid even minimal changes in the conductivity of the solution in the measuring cell, while keeping the sample wet. The conversion of measured streaming potential to zeta potential requires multiplication by the conductivity (Equation 1), thus any changes of solution conductivity translate into changes in zeta potential.

[b] Equation 1 is accurate to 1% when z is no more than 10% of the disk radius, $a/2$, which means for the sample of a = 25 mm, z should not be larger than 1.25 mm.

seen for the *Fucus vesiculosus* multilayer sample. However, apart from the first fucoidan layer, which gives rise to a zeta potential of approx. -44 mV, most of the values for the fucoidan layer are lower in the case of UP (-24 mV to -32 mV). In addition, the positive values observed for the multilayer with chitosan as the outer layer are greater in the $(UP/CH)_{10}$ multilayer stack (32 mV to 35 mV). The data indicate some variation in the build-up process for the two different fucoidan samples.

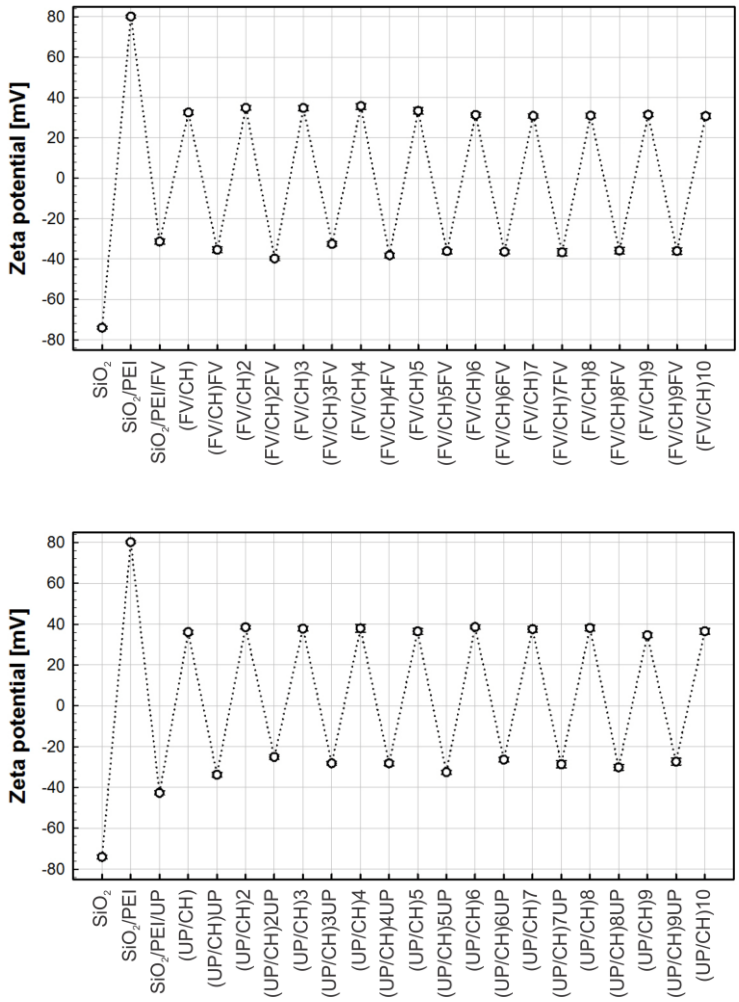

Figure S.1: Zeta potential measurements of multilayers of fucoidan and chitosan formed on silicon wafer substrates: top – FV/CH; and bottom – UP/CH. Measurements were performed in $1x10^{-3}$ M KCl at pH 6. Formation of multilayer from 500 ppm polymer solutions, 0.1 M KCl, pH 6.

Note: to prove that the two different cleaning procedures adopted in this study (one for QCM sensors, one for all other substrates – see methodology section in the main manuscript) do not have an impact on the measured zeta potential of silica surfaces, we have determined the zeta potential from streaming potential measurements for quartz discs cleaned in three different ways. For a quartz surface cleaned in 1 M KOH solution, the zeta potential (at 0.001 M KCl, pH 5.8) was -74.8 mV; for a quartz surface cleaned in piranha solution (one of the procedures used in the current work), the zeta potential (at 0.001 M KCl, pH 5.8) was -74.2 mV; and for a quartz surface cleaned in Hellmanex solution followed by the plasma cleaning (used for QCM sensors in the current work), the zeta potential (at 0.001 M KCl, pH 5.8) was -74.3 mV. This proves that the different cleaning methods do not affect the surface –OH groups (silanol groups), which are potential determining ions in the case of silica surfaces.

Spectroscopic Ellipsometry

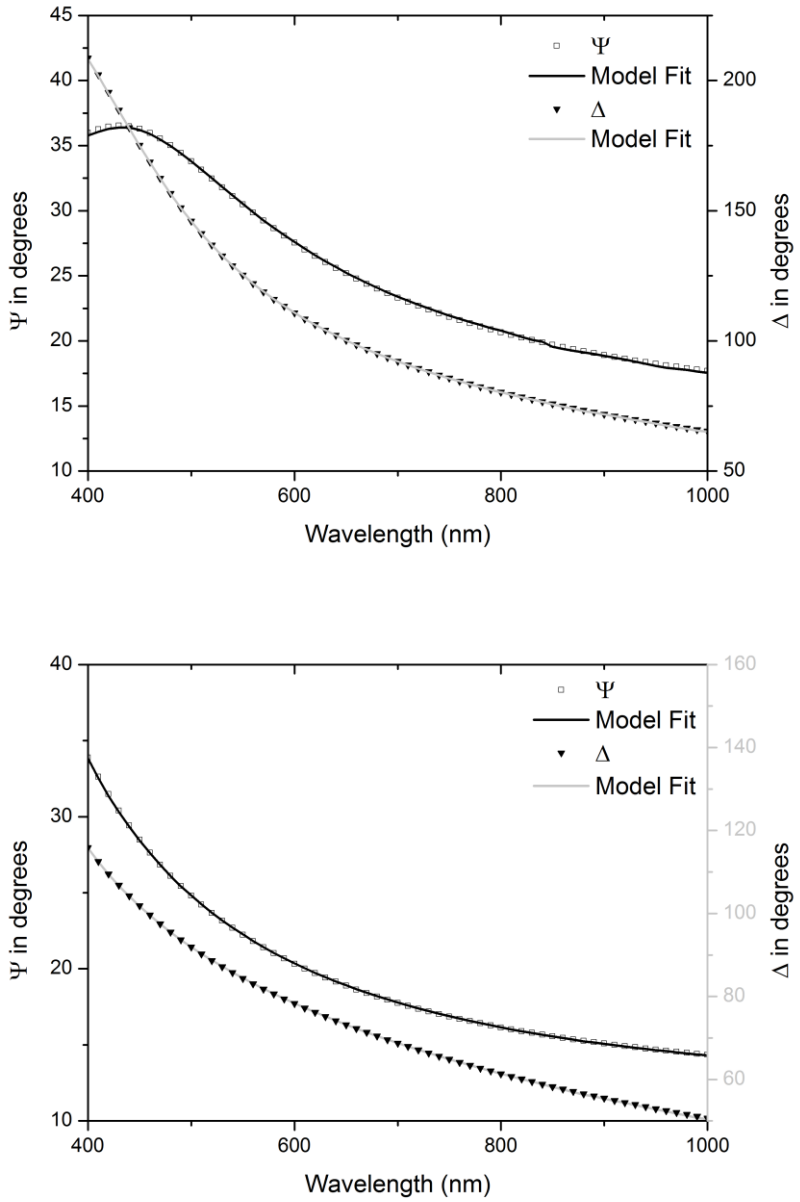

Figure S.2: Spectroscopic ellipsometry raw data (Ψ and Δ) for $(FV/CH)_{10}$ (top) and $(UP/CH)_{10}$ (bottom). Solid lines are model fit data based on a 4-layer model, with the PEM described by a Cauchy layer.

Table S.1: Ellipsometric thickness and adsorbed mass (determined from the de Feijter equation) for multilayer build-up of $(FV/CH)_{10}$ and $(UP/CH)_{10}$ PEMS on silicon wafer substrates.

	FV/CH		UP/CH	
	Thickness (nm)	Mass (ng/cm2)	Thickness (nm)	Mass (ng/cm2)
PEI	1.5	116	1.4	107
1	4.1	322	3.4	270
2	5.5	434	4.6	364
3	7.8	615	6.6	518
4	13.2	965	8.2	641
5	20.0	1240	10.5	822
6	23.5	1623	12.4	1225
7	33.1	2026	17.9	1501
8	36.1	2574	21.0	1845
9	51.1	3093	29.5	2203
10	53.8	3777	32.4	2651
11	73.5	4408	42.8	3099
12	75.7	5132	45.6	3625
13	97.1	5808	56.5	4133
14	99.4	6547	59.8	4662
15	120.8	7309	70.7	5210
16	124.2	8013	74.3	5718
17	143.8	8777	84.6	6238
18	148.7	9484	89.0	6729
19	166.7	10267	99.0	7299
20	170.9	10805	103.7	7779

Quartz Crystal Microbalance

Adsorption – All Overtones

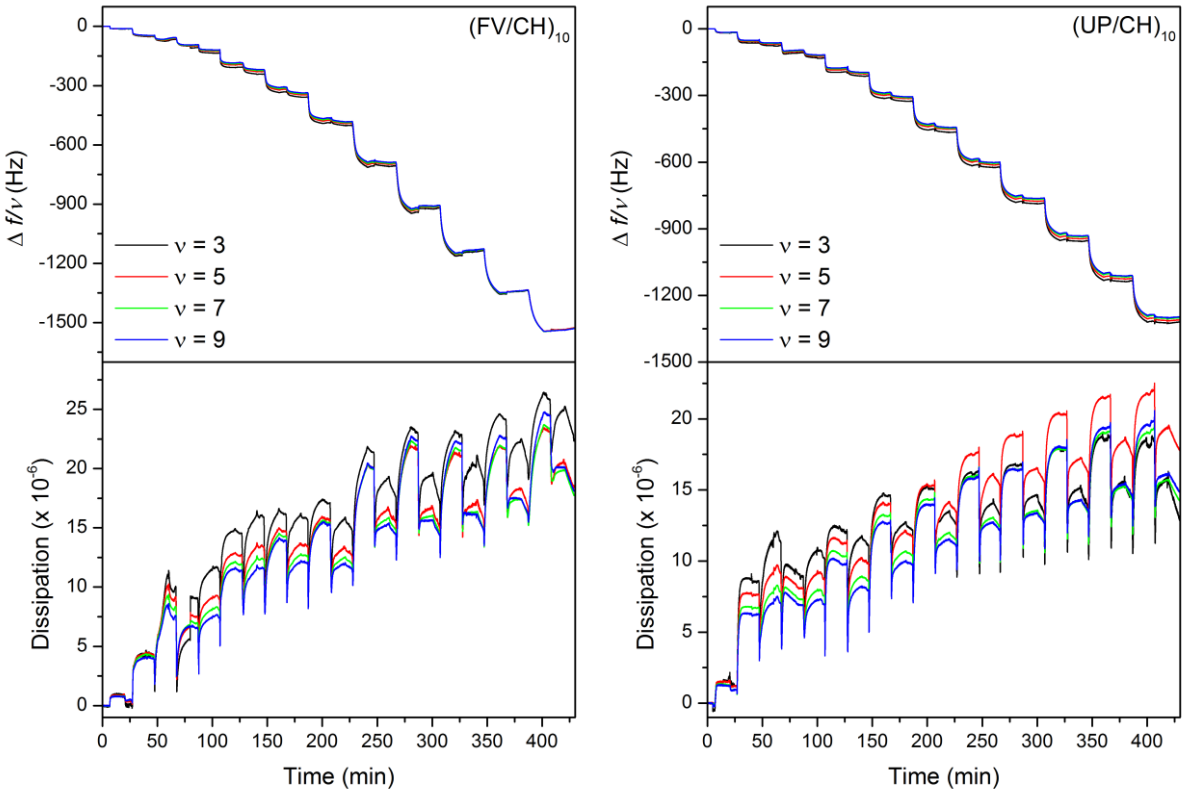

Figure S.3: QCM-D data for the formation of $(FV/CH)_{10}$ (left) and $(UP/CH)_{10}$ (right). Non-normalized frequency change data for overtones 3, 5, 7, and 9, and dissipation change for the same overtones are given in each plot.

QCM-D Voigt Fitting

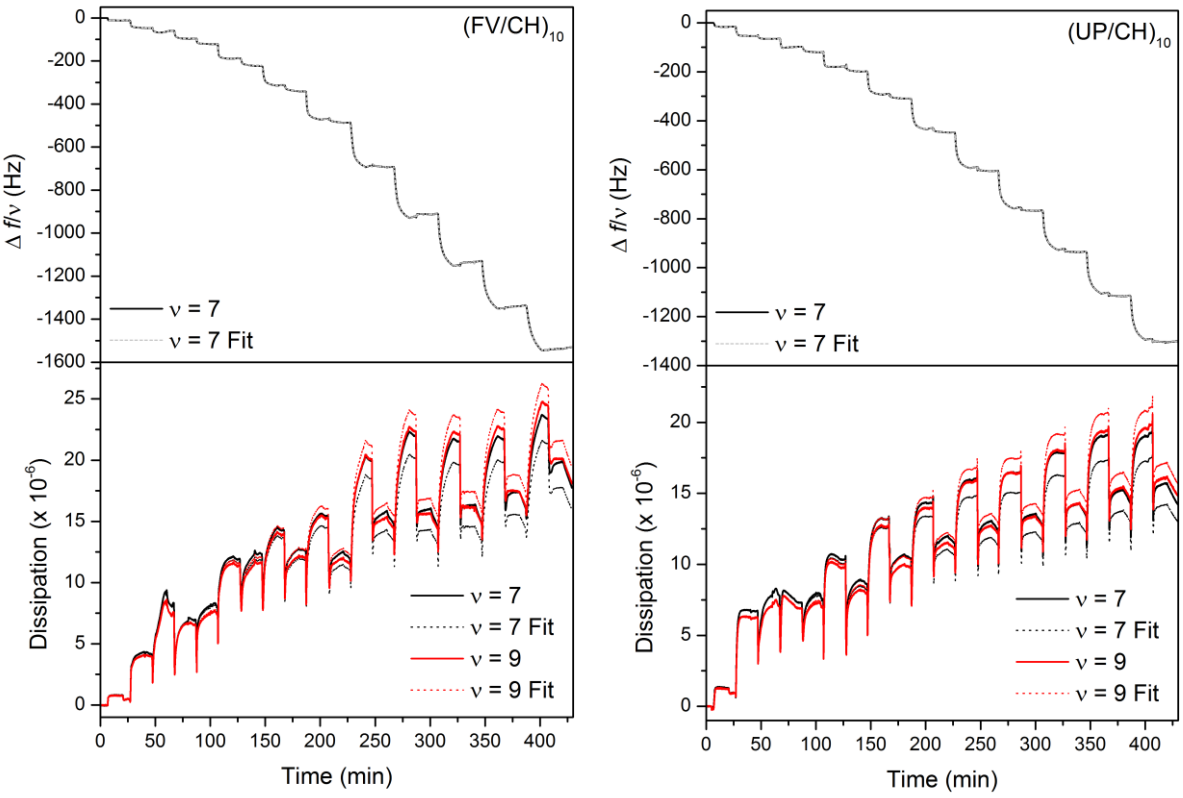

Figure S.4: QCM-D data for the formation of $(FV/CH)_{10}$ (left) and $(UP/CH)_{10}$ (right). Frequency (7^{th} overtone) and dissipation (7^{th} and 9^{th} overtone) are used to perform Voigt fitting for the determination of the viscoelastic properties of the films. Tabulated data from the Voigt fitting is presented in the main manuscript.

AFM Imaging Methodology

The film thickness was measured to determine the growth characteristics of the Fucoidan-Chitosan multilayers. The direct film thickness measurement was carried out using AFM scratch-and-scan method. In this method, a small part of the film is removed (using a scalpel blade) and a 'step' between the smooth substrate (silicon wafer with removed PEM film) and the PEM film is imaged with an AFM. An optical microscope image of the scratched area on a PEMs film is shown in Figure S.1 together with its AFM micrograph. The area with the removed PEM film can be clearly seen due to its smoothness. The cross section of the PEMs profile thickness was then extracted from AFM height image. To exclude the possibility of silicon wafer damage by the scalpel blade scratch, a clean silicon wafer was scratched with the scalpel blade and 5 x 5 μm^2 AFM image was taken. The height images show no visible damage.

To determine an average film thickness, h_a, height differentials (height of every pixel in image relative to the height of the bare substrate) were averaged to produce histograms of each scan, with the software determining the number average height value. To ensure that measurements from the bottom of the scratch (the substrate) didn't lower the calculation for the film thickness, the areas of scratches was almost entirely excluded. The reported h_a value were determined using height analysis of different areas of three independent samples for each case studied. AFM was also used to calculate peak-to-valley (PTV) and root mean square (R_{rms}) roughness.

The film height and roughness measurements require some prior processing due to sample misalignment (image tilt) and/or effects coming from the piezoelectric scanners employed (image bow). These problems can be easily removed by fitting the image to a surface defined by a polynomial [c]. Since the 5 x 5 μm^2 scans taken by AFM are less prone to the presence of image bow all the AFM images were only fitted with a first-order plane fit (to remove the image tilt) calculated from an image area of the silicon surface that did not include the step.

[c] The planefit procedure calculates a single polynomial fit for the entire image and then subtracts the polynomial fit from the image.

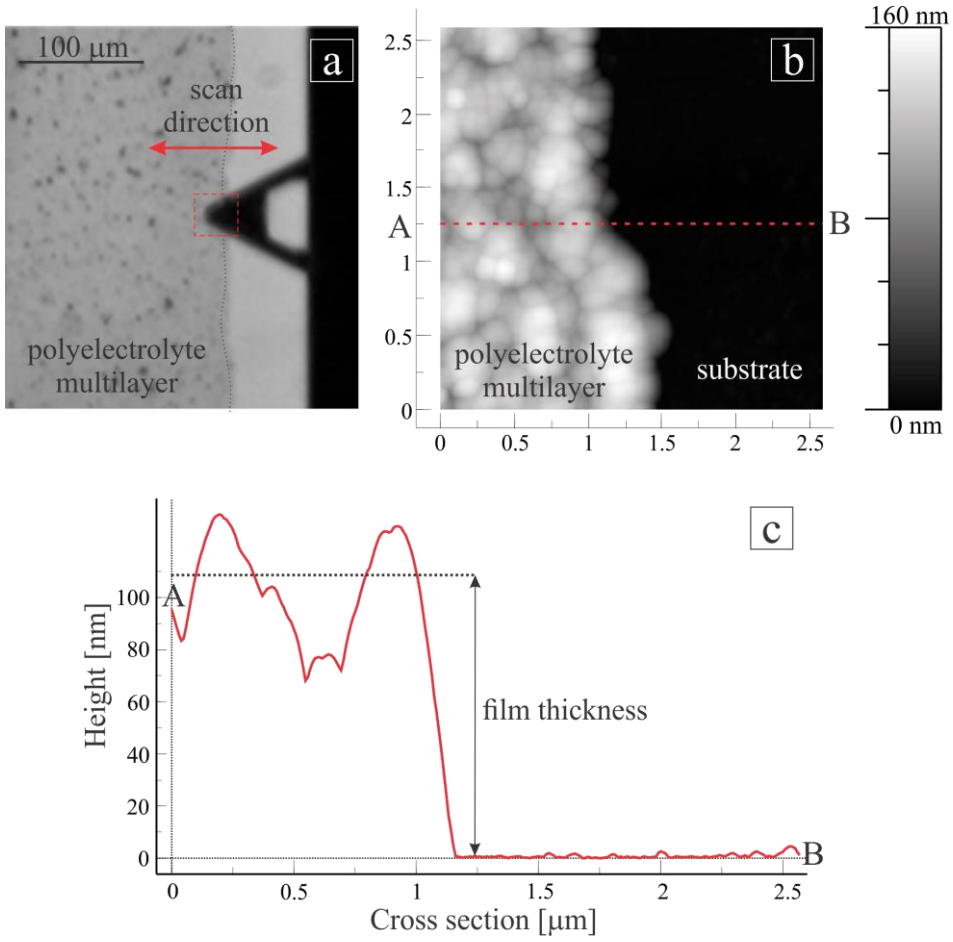

Figure S.5: (a) Top camera view of the cantilever and the scratch on the PEM film (delimited with the dashed line). The red square indicates the scan area (out of scale). (b) 2-D AFM image taken across the scratch showing higher (brighter) features forming the PEMs film, and the dark flat region representing the silicon wafer with the PEM film removed. The grey scale bar shows the height. (c) Height profile through the cross-section line (A‑B) of a PEM film.

AFM Imaging of Fucoidan/Chitosan (2, 4, 6, 8, and 10 Bilayers)

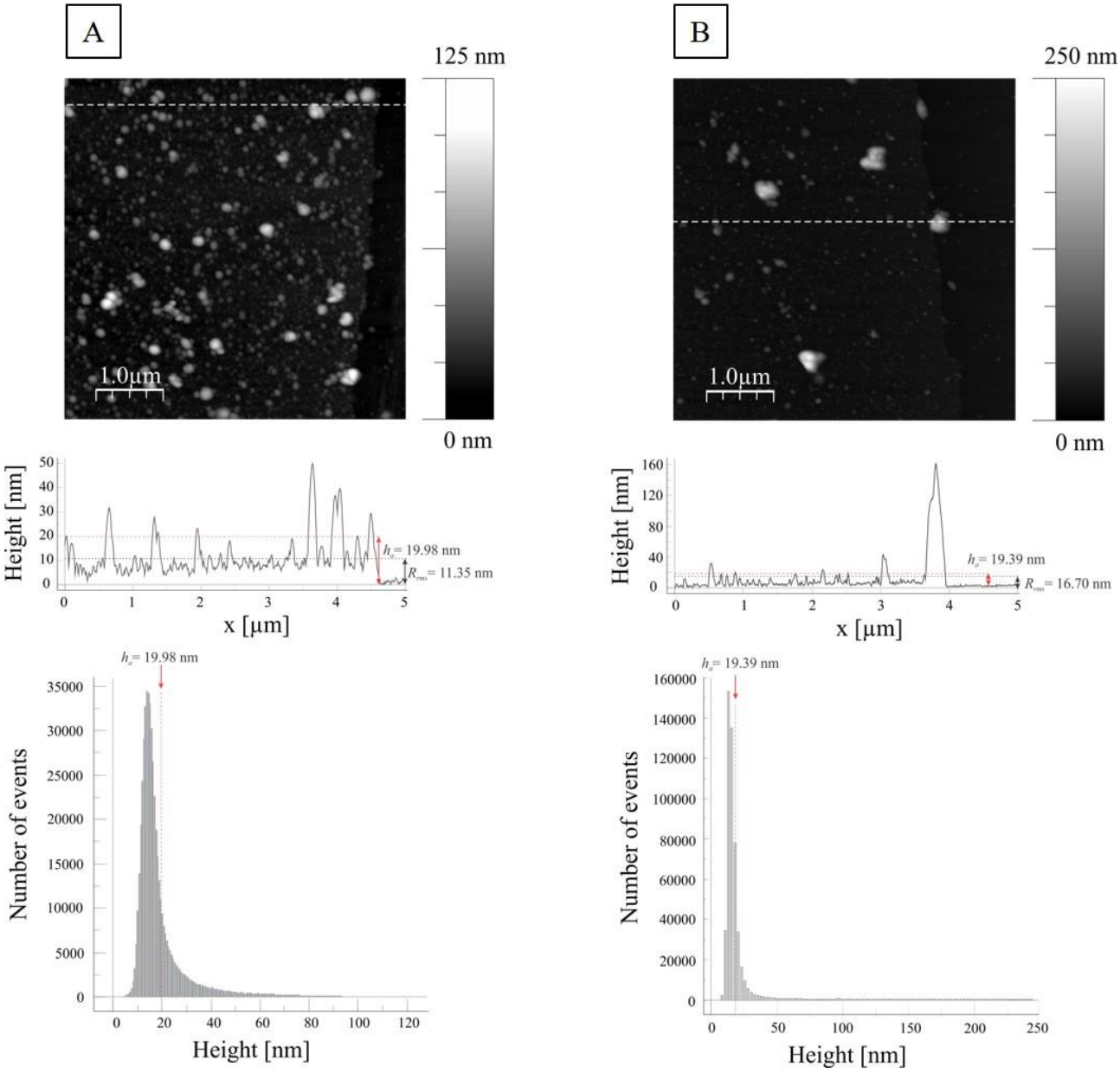

Figure S.6: The first row contains AFM height images (5×5 µm^2) of a 2 bilayer sample formed with: (A) FV, and (B) UP. The topography of the images differs between two fucoidans. FV forms larger features. In addition, the size distribution is much narrower in comparison to UP. The middle row shows the cross section of the topographic images across the dashed lines in AFM height images for both fucoidans. While for FV the height of the features is quite similar and spans over quite narrow size range from 5 to 95 nm, for UP the size distribution is much wider, from 5 to 245 nm. In addition, for UP the number of counts for heights smaller than the average height is higher by factor of ~ 3, but a few features as tall as 160 nm are also present. The bottom row presents relative height histograms for AFM topographic images. The average height values calculated from the histograms for both fucoidans are similar.

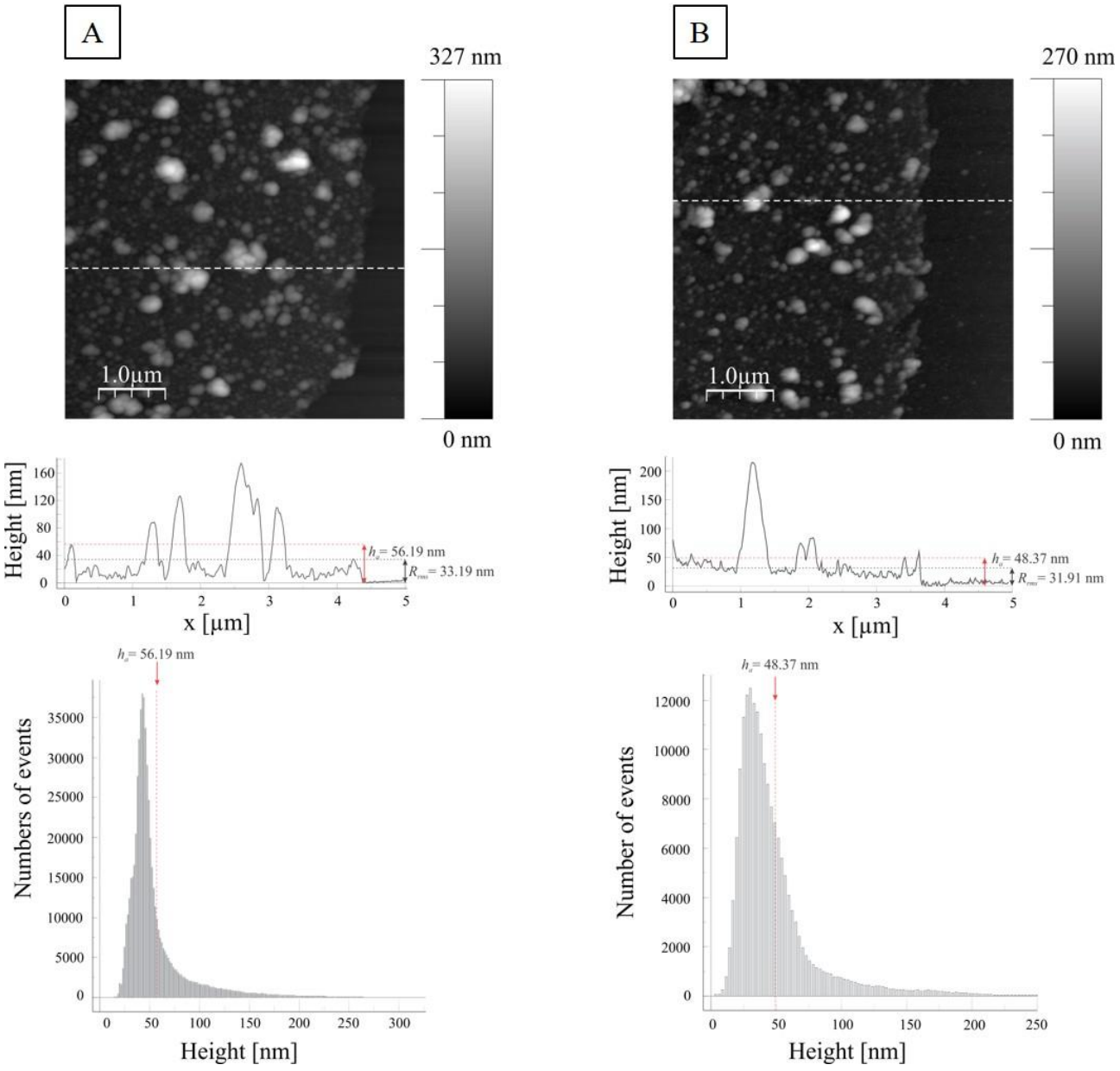

Figure S.7: The first row contains AFM height images (5×5 µm^2) of a four bilayer sample formed with: (A) FV, and (B) UP. The topography of PEMs is more similar than the topography for a two bilayer sample for two fucoidans. Both FV and UP have a mixture of both small and large features in the multilayer. The middle row shows the cross section of the topographic images across the dashed lines in AFM height images for both fucoidans. Cross sections are similar for both fucoidans. The bottom row presents relative height histograms for AFM topographic images. The average height values calculated from the histograms for both fucoidans are similar. The size distribution is similar for both samples: 5 to 270 nm for FV and 5 to 250 nm for UP.

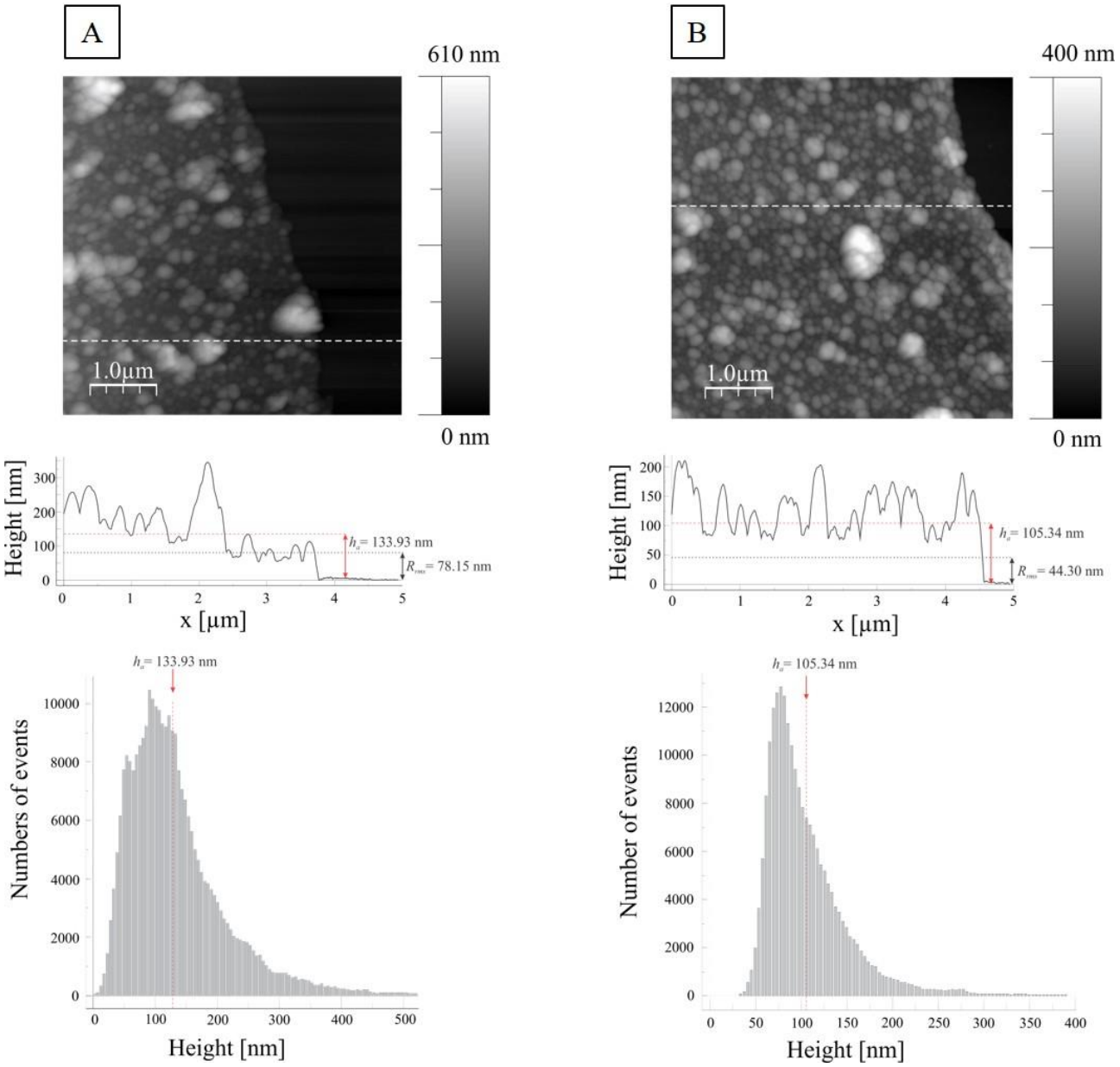

Figure S.8: The first row contains AFM height images (5×5 µm^2) of a six bilayer sample formed with: (A) FV, and (B) UP. The topography of the PEMs differs between two fucoidans. FV forms larger and higher features of much more differentiated size. The middle row shows the cross section of the topographic images across the dashed lines in AFM height images for both fucoidans. The bottom row presents relative height histograms for AFM topographic images. The average height values calculated from the histograms are higher by around 30 % for FV. The size distribution is much wider for FV and it spans over 5 – 500 nm height range, while UP forms features more uniform in size: 30 – 390 nm.

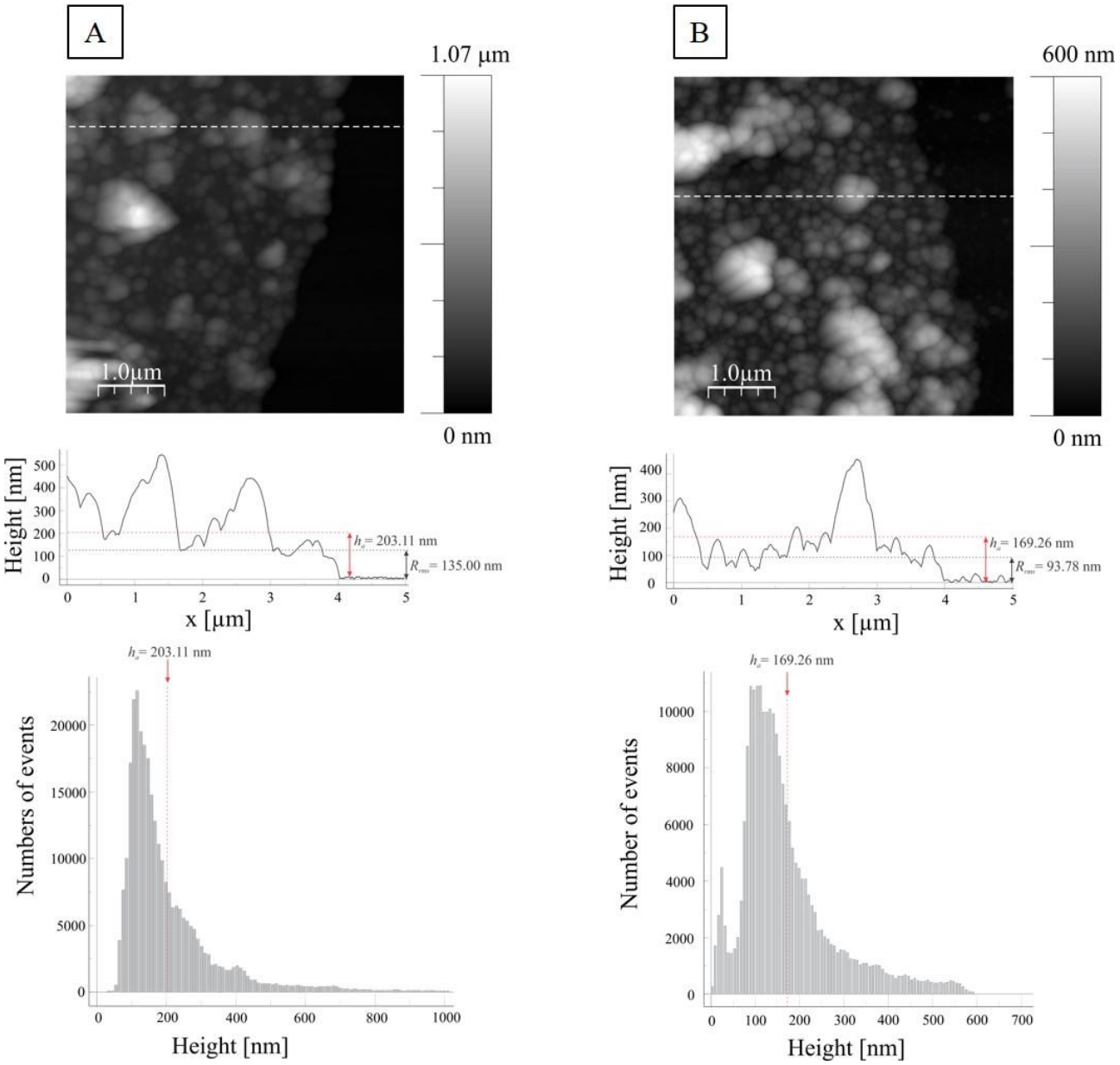

Figure S.9: The first row contains AFM height images (5×5 µm^2) of an eight bilayer sample formed with: (A) FV, and (B) UP. The topography of PEMs differs between two fucoidans. FV forms larger and higher features of much more differentiated size. The middle row shows the cross section of the topographic images across the dashed lines in AFM height images for both fucoidans. The bottom row presents relative height histograms for AFM topographic images. The average height values calculated from the histograms are higher by around 20 % for FV. The size distribution is much wider for FV and it spans over 5 – 1050 nm height range, while UP forms features more uniform in size: 5 – 580 nm.

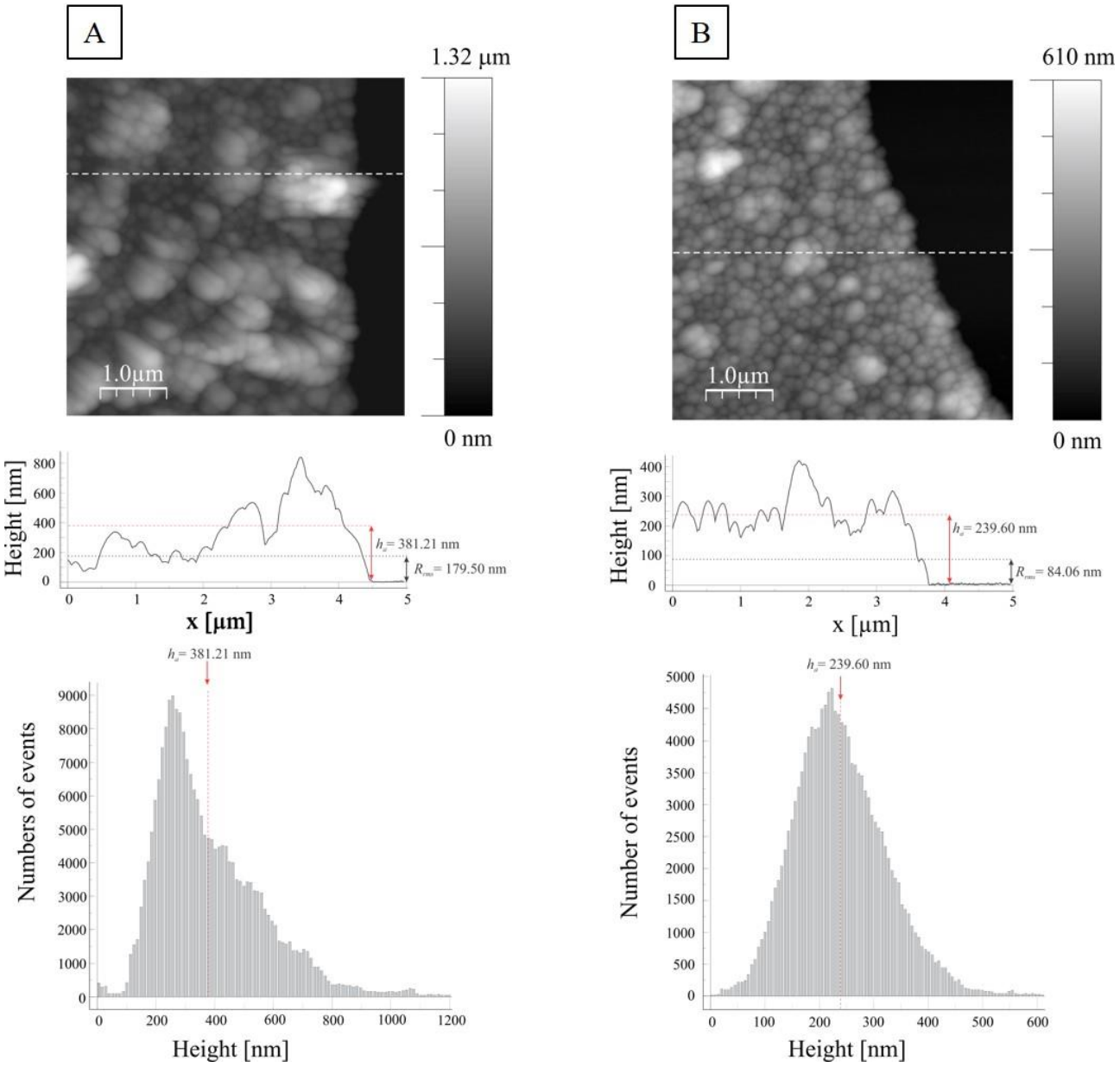

Figure S.10: The first row contains AFM height images (5×5 µm^2) of a ten bilayer sample formed with: (A) FV, and (B) UP. The topography of PEMs differs significantly between two fucoidans. FV forms highly non-uniform film containing larger and higher features. The middle row shows the cross section of the topographic images across the dashed lines in AFM height images for both fucoidans. The bottom row presents relative height histograms for AFM topographic images. The average height values calculated from the histograms are higher by around 60 % for FV. Similarly as for lower bilayer numbers, the size distribution is much wider for FV and it spans over 5 – 1200 nm height range, while UP forms features more uniform in size: 5 – 610 nm.

Table S.2 Film roughness and thickness of (FV/CH) polyelectrolyte multilayers.

Number of FV/CH bilayer	R_{rms} [nm]	PTV [nm]	h_a [nm]
2nd	11.35	125.48	19.98
4th	33.19	324.99	56.19
6th	78.15	523.45	133.93
8th	135.00	1025.10	203.11
10th	179.00	1206.21	381.21

Table S.3 Film roughness and thickness of (UP/CH) polyelectrolyte multilayers.

Number of FV/CH bilayer	R_{rms} [nm]	PTV [nm]	h_a [nm]
2nd	16.70	248.42	19.39
4th	31.91	267.01	48.37
6th	44.30	400.12	105.34
8th	93.78	587.11	169.26
10th	84.06	613.90	239.60

X-ray Photoelectron Spectroscopy

Survey Scans

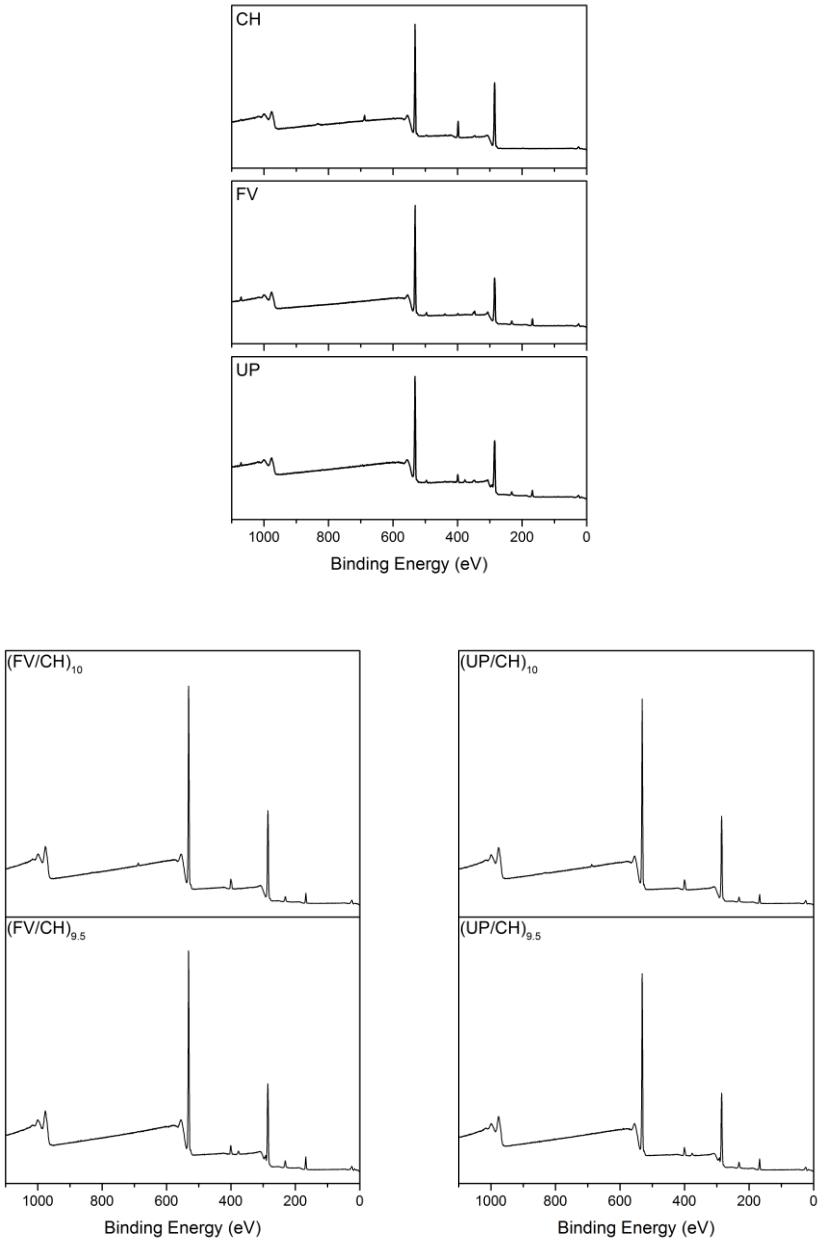

Figure S.11: XPS survey scans for $(FV/CH)_{10}$, $(UP/CH)_{10}$, $(FV/CH)_{9.5}$, $(UP/CH)_{9.5}$, in addition to CH, FV, and UP.

XPS High Resolution Scans

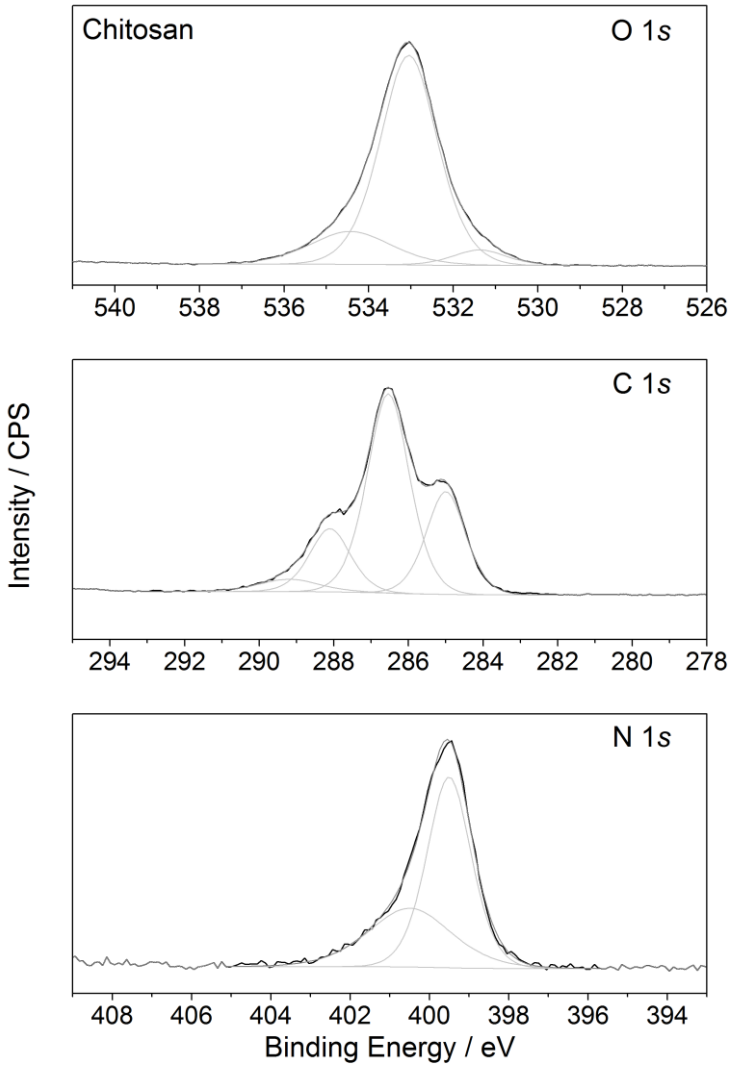

Figure S.12: XPS high resolution scans for O 1*s*, C 1*s*, and N 1*s* photoemission peaks of bulk chitosan.

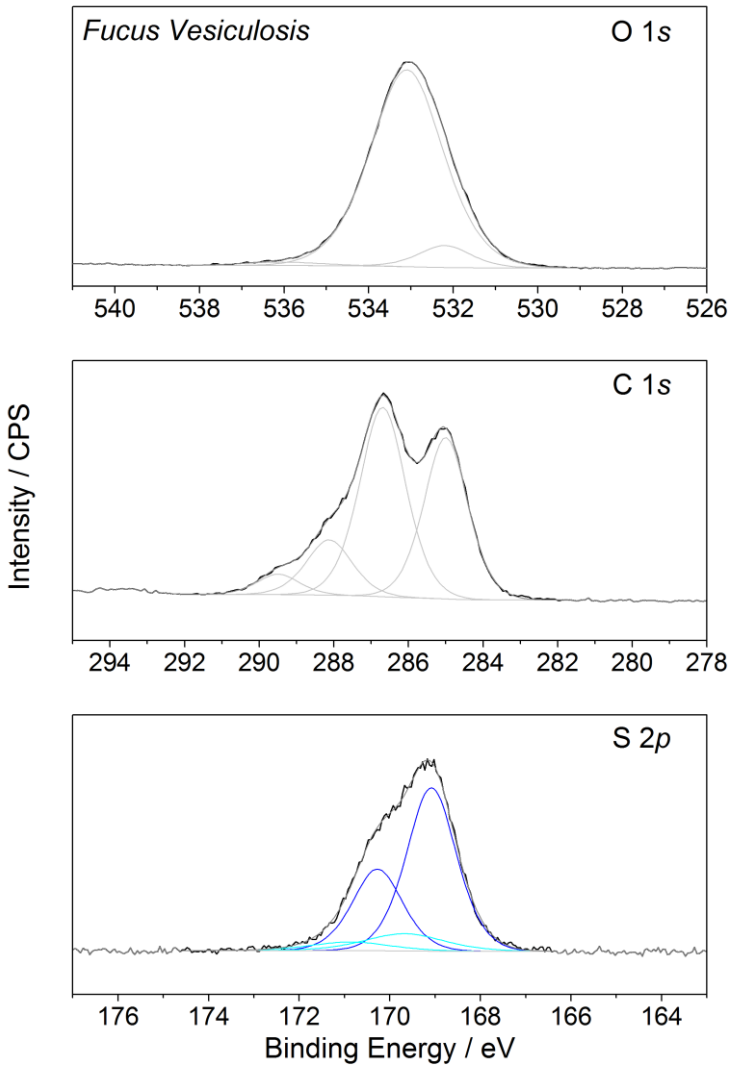

Figure S.13: XPS high resolution scans for O 1*s*, C 1*s*, and S 2*p* photoemission peaks of bulk *Fucus Vesiculosis*.

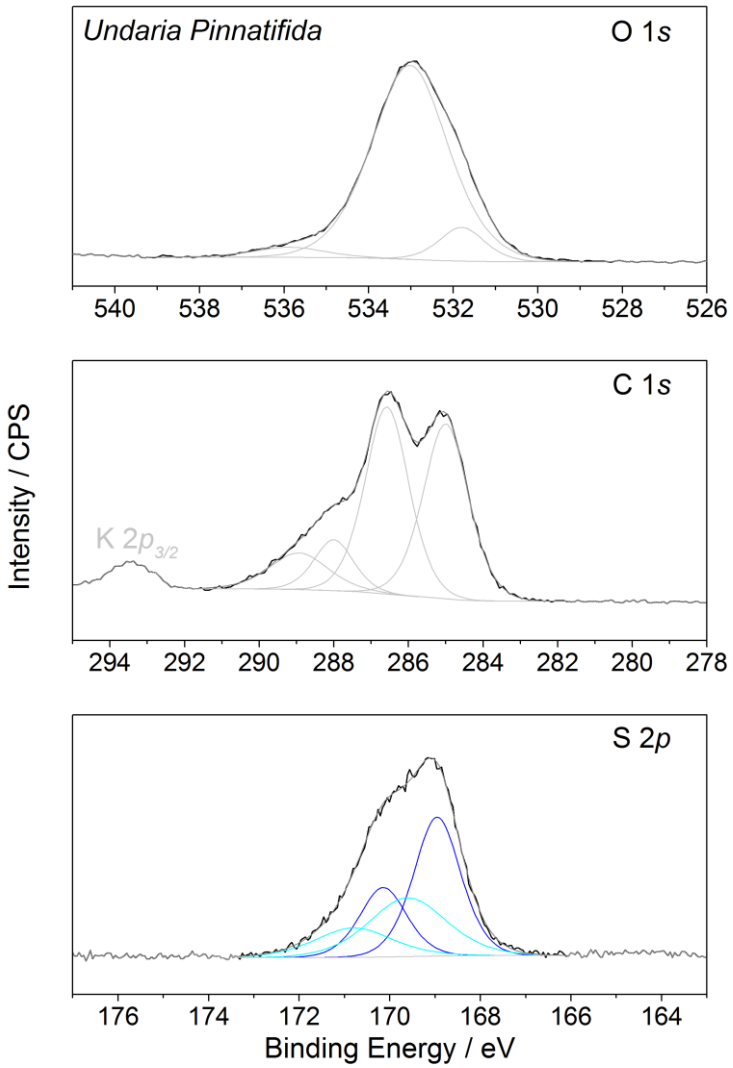

Figure S.14: XPS high resolution scans for O 1*s*, C 1*s*, and S 2*p* photoemission peaks of bulk *Undaria Pinnatifida*.

Table S.4: Surface atomic concentrations for CH, FV, and UP.

Elements	CH	FV	UP
O	30.4	37.1	34.1
C	62.4	56.8	57.9
N	6.8	0.6	3.9
S	-	3.9	3.3
Ca	0.3	1.1	-
Na	0.1	0.5	0.3
K	-	-	0.5

Table S.5: XPS peak positions, relative abundance, and peak widths for the components of the C 1*s*, O 1*s*, and N 1*s* spectra for bulk chitosan.

Element	**Binding Energy**	**Abundance (%)**	**FWHM (eV)**	**Assignment**
C 1*s*	285.0	26	1.2	C-H
	286.5	53	1.3	C-OH, C-O, C-N
	288.1	16	1.3	O-C-O
	289.2	3	1.9	O-C=O
O 1*s*	531.4	5	1.5	-NH-C=O
	533.0	78	1.6	C-O/C=O/O-C-O
	534.4	17	2.2	Physisorbed H_2O
N 1*s*	399.5	63	1.3	$-NH_2$, -NH-C=O
	402.2	37	2.4	$-NH_3^+$

.

Table S.6: XPS peak positions, relative abundance, and peak widths for the components of the C 1*s*, S 2*p*, and O 1*s* spectra for bulk *Fucus Vesiculosis* and *Undaria Pinnatifida*.

	Fucus Vesiculosis			***Undaria Pinnatifida***			
Element	**Binding Energy**	**Abundance (%)**	**FWHM (eV)**	**Binding Energy**	**Abundance (%)**	**FWHM (eV)**	**Assignment**
C 1*s*	285.0	37	1.4	285.0	39	1.4	C-H
	286.7	46	1.4	286.6	40	1.6	C-OH, C-O
	288.2	13	1.4	288.0	10	1.2	O-C-O
	289.3	4	1.3	288.9	11	1.8	O-C=O
S 2*p*$_{3/2}$	169.1	85	1.3	169.0	59	1.2	SO_3^-
	169.7	15	2.0	169.6	41	2.0	interacting SO_3^-
O 1*s*	532.2	7	1.5	531.8	9	1.3	SO_3^-
	533.1	91	2.0	533.0	87	2.1	C-O/C=O/O-C-O
	536.0	2	2.1	535.9	4	1.9	Physisorbed H_2O [a]

[a] high binding energy for physisorbed water is attributable to the presence of water clusters in the material [3]

References

1. P. J. Sides, J. Newman, J. D. Hoggard and D. C. Prieve, *Langmuir*, 2006, **22**, 9765-9769.
2. P. J. Scales, F. Grieser, T. W. Healy, L. R. White and D. Y. C. Chan, *Langmuir*, 1992, **8**, 965-974.
3. J. M. C. Lourenço, P. A. Ribeiro, A. M. Botelho do Rego and M. Raposo, *J. Colloid Interface Sci.*, 2007, **313**, 26-33.